

Real-Time Monitoring of Growth and Orientational Alignment of Pentacene on Epitaxial Graphene for Organic Electronics

Martin Hodas,^{*,†,‡,§} Peter Siffalovic,^{‡,§,¶} Peter Nádaždy,[‡] Nad'a Mrkyvková,[‡] Michal Bodík,^{‡,§} Yuriy Halahovets,[‡] Giuliano Duva,^{†,§} Berthold Reisz,[†] Oleg Konovalov,[§] Wiebke Ohm,^{||} Matej Jergel,^{‡,§} Eva Majková,^{‡,§,¶} Alexander Gerlach,[†] Alexander Hinderhofer,^{†,§} and Frank Schreiber[†]

[†]Institut für Angewandte Physik, Universität Tübingen, Tübingen 72076, Germany

[‡]Institute of Physics, Slovak Academy of Sciences, Bratislava 84511, Slovakia

[§]Centre of Excellence for Advanced Materials Application, Bratislava 84511, Slovakia

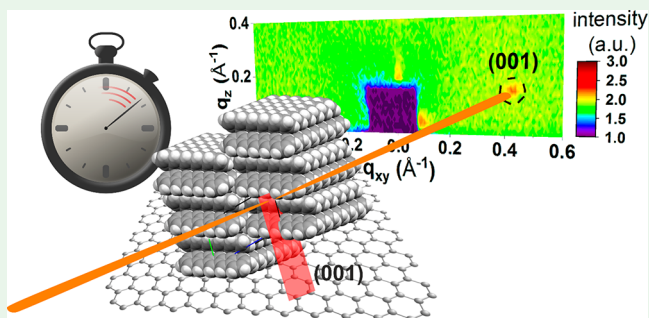
^{||}European Synchrotron Radiation Facility, Grenoble 38000, France

[¶]Photon Science, Deutsches Elektronen-Synchrotron (DESY), Hamburg 22607, Germany

Supporting Information

ABSTRACT: The interaction between a graphene layer and pentacene (PEN) molecules leads to the formation of a *lying-down* phase, which can improve charge transport for organic vertical field effect transistors and enhance the optical absorption for increased light harvesting in organic solar cells. Here, we present a comprehensive study of PEN growth on epitaxial graphene on silicon carbide (SiC). Simultaneous grazing-incidence small- and wide-angle X-ray scattering (GISAXS/GIWAXS) were used in situ for real-time monitoring of the PEN crystal growth with millisecond time resolution to identify *two* distinct anisotropic growth stages after the nucleation of the first monolayer (ML). In the first stage up to 1.5 nm, we observe rapid growth of pentacene domains along the (010) and (001) facets. This growth behavior is saturating after 1.5 nm. In a second stage, this is followed by continuous lateral crystal growth in only one in-plane direction (100) forming needle-shaped domains. In the second stage, an uninterrupted linear growth of the *lying-down* PEN phase is found based on the (001) diffraction up to 15 nm. Ex situ atomic force microscopy and polarized confocal Raman microscopy were used to further support the real-time observations of aligned PEN films on graphene.

KEYWORDS: pentacene, epitaxy, graphene, X-ray scattering, growth, AFM, polarized Raman



INTRODUCTION

The combination of organic semiconductors with two-dimensional (2D) materials¹ holds the promise of new emerging applications in organic electronics.² In the past decade, the ability of molecular alignment control by templating the substrates with 2D materials was reported.^{3–15} Pentacene (PEN) is a prototypical organic semiconductor used in OFETs and organic solar cells for its well-known structure,¹⁶ optical^{17,18} and electronic properties. The conventional “*standing-up*” thin film phase of PEN on oxide substrates can be manipulated toward a “*lying-down*” phase on graphene. Considering the strong anisotropies of crystalline small-molecule semiconductors,^{19–22} it is obvious that this “orientation engineering” can have a strong influence on the vertical charge transport and light absorption, which, in turn, are key parameters for applications. Indeed, highly oriented PEN films on graphene were shown to improve the light harvesting in organic solar cells.¹¹ The capability to control the molecular orientation is thus vital for coming generations of

organic device applications, such as also vertical field effect transistors.^{2,23} It is therefore particularly important that the epitaxial growth of organic molecules on 2D materials can be employed as a template for molecular epitaxy in more complex organic heterostructures.²⁴

A large number of studies were devoted to understanding the underlying mechanisms of molecular-level control of small molecules on graphene.^{15,25–27} The real-space studies relying on scanning probe microscopies revealed initial stages of nucleation and submonolayer growth of PEN on graphene^{3,7,8,10,12} and on highly ordered pyrolytic graphite (HOPG).^{28,29} A special class of real-time experiments on molecular growth of small semiconducting molecules on graphene were conducted using low-energy electron microscopy (LEEM) and its reciprocal space counterpart, i.e., micro low-

Received: March 23, 2018

Accepted: May 31, 2018

Published: May 31, 2018

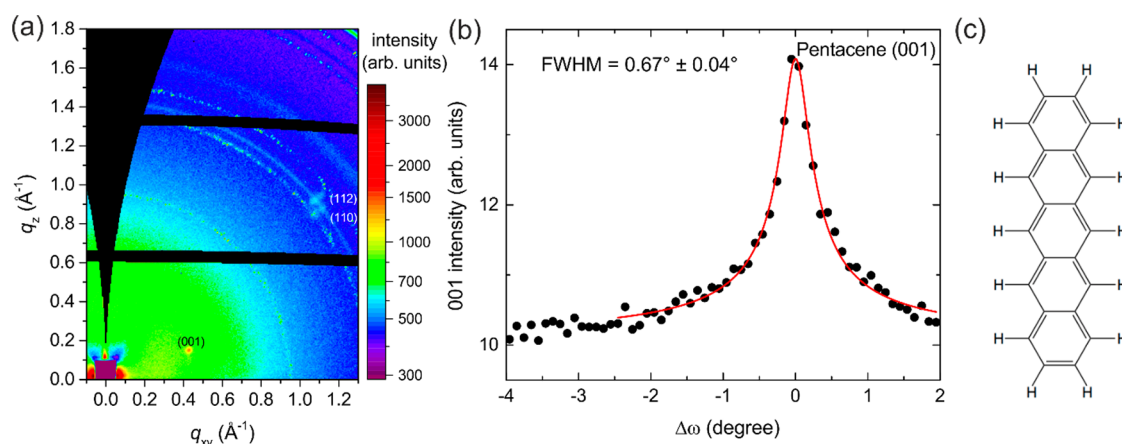


Figure 1. (a) Reciprocal space map of 15 nm PEN film grown on epitaxial graphene at a substrate temperature of 50 °C and deposition rate of 1.38 Å/min. The diffraction rings belong to the beryllium entry and exit window of the vacuum chamber (at $q = 0.95, 1.36, 1.41, 1.50 \text{ \AA}^{-1}$). (b) Azimuthal scan of the (001) diffraction spot of PEN. (c) Molecular structure of PEN.

energy electron diffraction (μ LEED).^{6,30} Real-time optical spectroscopic experiments on the molecular growth of organic molecules have been performed to better understand their structural and electronic properties.^{31–33} Grazing-incidence wide-angle X-ray scattering (GIWAXS) became the standard characterization technique to verify the molecular alignment in PEN thin films.^{4,13,34} Importantly, the high brilliance of synchrotron X-ray radiation sources makes real-time and in situ experiments of molecular thin film growth feasible.^{35–38} The growth modes of various organic molecules were studied in-depth by employing real-time GIWAXS and X-ray reflectivity (XRR).^{35,36,39,40} Real-time experiments are key for a better understanding of the diffusion of molecules on the surface as well as the time evolution of structure, electronic, and optical properties, since they capture possibly transient behavior during growth and also different kinetic growth stages. Various strategies for real-time X-ray scattering have been developed. One possible technique based on the time evolution of anti-Bragg intensity has been developed in order to track the layer-by-layer growth (or deviations from this) of PEN and similar molecules on oxide substrates.^{41–46} Grazing-incidence small-angle X-ray scattering (GISAXS), a technique complementary to GIWAXS, can recover the shape and distribution of growing molecular islands at submicrometer scale in real time.^{47–53}

Here, we report a comprehensive study of PEN crystal growth on epitaxial graphene on single crystalline SiC. The simultaneous real-time GIWAXS complemented by GISAXS enables tracking of molecular orientation, crystal orientation, and island size on the nanoscale with millisecond temporal resolution. The large-scale monocrystalline graphene on SiC is a vital component, which facilitates the monitoring of oriented growth of PEN crystals. In this specific case, the c -axis orientation of growing PEN crystals adopts the six-fold symmetry of underlying graphene on a macroscopically large scale, which makes it possible to study the growth of specific crystal facets by GISAXS. On the other hand, the polycrystalline chemical vapor deposition (CVD) grown graphene used in other works supports only time-resolved GIWAXS studies due to a large number of randomly oriented graphene grains. Our experiments revealed continuous growth of an oriented PEN “lying-down” phase with crystallographic orientation inherited from the underlying graphene substrate. The nanoscale PEN crystals exhibit preferential growth of (100) facets, which leads

to the formation of highly anisotropic elongated shapes of PEN islands on graphene. The crystal growth along the (001) and (010) facets of the macroscopic PEN crystal shows rapid growth during the first few nanometers, whereas second stage growth along these facets saturates and continues only the crystal growth along the (100) facets. Our findings are further supported by ex situ experiments using atomic force microscopy (AFM) and polarized confocal Raman microscopy (CRM). The present study clearly demonstrates the prospects of simultaneous GI-SAXS/WAXS measurements to monitor growth of semiconducting molecular crystals on 2D substrates. The results were only possible via real-time investigations, as they allow us to continuously monitor growth of small organic molecules on substrate starting from the very beginning and see all regimes of the growth.

RESULTS AND DISCUSSION

Postgrowth GIWAXS Studies. The 4H-SiC(0001) substrate enables growth of monocrystalline graphene over a large area ($>100 \text{ mm}^2$).^{3,8,54–56} This is essential for grazing-incidence studies, where the impinging X-ray beam at an angle of incidence close to the critical angle for total X-ray reflection ($\sim 0.1\text{--}0.2^\circ$) probes a surface area of several square millimeters. The large area facilitates excellent statistics of the crystallinity and morphology of organic thin films. Moreover, the well-defined orientation⁵⁵ of the graphene unit cell with respect to SiC supports precise alignment of the graphene lattice and exact determination of the PEN unit cell orientation. Figure 1a shows the reciprocal space map (RSM) of a PEN film with the equivalent thickness of 15 nm recorded in GIWAXS mode.

Due to island growth (Volmer–Weber mode) of oriented PEN crystals on graphene,⁷ we adopt a measure of film thickness in effective nanometers of PEN deposited on a reference Si/SiO₂ sample (Si wafer with native amorphous oxide layer), which is known to support the “thin film” PEN phase.⁵⁷ The precise deposition rate on the Si/SiO₂ substrate was calibrated ex situ, employing spectroscopic ellipsometry,¹⁸ and was complemented by quartz crystal microbalance (QCM) measurements in all X-ray scattering experiments. In stark contrast to the RSMs of PEN thin films grown on polycrystalline CVD graphene, only a few diffraction spots, the (001) Bragg peak being the dominant one, are visible (Figure 1).

The (001) lattice planes are tilted by approximately 18° with respect to the sample surface as reported by similar measurements on CVD graphene.^{4,13} The azimuthal scan of the (001) diffraction spot (Figure 1b) around the sample normal reveals a Lorentzian-shaped profile with a width of $0.67 \pm 0.04^\circ$ (fwhm), which points to highly oriented single crystal PEN islands on the graphene template. Apart from the strong (001) diffraction, two faint (1 $\bar{1}$ 0) and (112) diffraction spots from PEN are visible. These diffractions originate from the symmetry-equivalent orientations of PEN islands. The six-fold symmetry of the underlying graphene lattice supports preferential growth of six differently oriented PEN islands. While one particular orientation of PEN satisfies the Bragg condition for the observation of the (001) diffraction spot, it can be shown that sets of PEN crystals rotated by 120° and 300° correspond to the (1 $\bar{1}$ 0) and (112) diffraction spots, respectively (Figure S1). In order to verify the six-fold symmetry of the PEN film inherited from graphene, we have rotated the sample by 60° and validated the existence of (001) Bragg reflection from PEN film.

The positions of the observed diffraction spots can be adequately described by the single crystal phase of PEN reported by Mattheus et al.⁵⁸ The hexagonal unit cell of the graphene lattice is rotated by 30° off the SiC hexagonal unit cell⁵⁵ as shown in Figure 2. Our ex situ measurements confirm

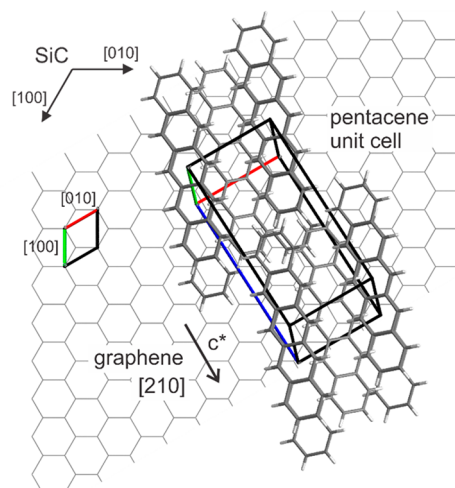


Figure 2. Orientation of the PEN unit cell with respect to underlying graphene lattice. The unit cell vectors **a**, **b**, and **c** are denoted by red, green, and blue colors, respectively.

that the reciprocal c^* axis of the PEN crystal is aligned along the graphene [210] (armchair) direction and is tilted by 18° from the graphene surface (Figure 2). The crystallographic axis **a** of the PEN unit cell lies in the graphene plane. Adopting the PEN molecular orientation within the unit cell as determined by Mattheus et al.,⁵⁸ we can conclude that the long PEN axis is not aligned along the [100] (zigzag) graphene direction as in the case of a PEN ML,⁸ but it is rather tilted by 12° with respect to the zigzag direction (Figure 2). A comparable inclination of the long molecular axis was reported for graphene¹⁰ and HOPG²⁹ consistently using scanning tunneling microscopy (STM). The energy minimization drives the reorientation²⁹ of the long molecular axis because of different interaction energies between pentacene–graphene and pentacene–pentacene molecules.

Time-Resolved GIWAXS Studies. High-brilliance synchrotron radiation allows time-resolved measurements of temporal changes in GIWAXS RSMs of growing PEN films. In our study, we focused on the tracking of the integral intensity and the profile of the (001) diffraction spot (Figure 1a) in reciprocal space as a function of growing film thickness. Figure 3 shows the evolution of the (001) integral intensity and

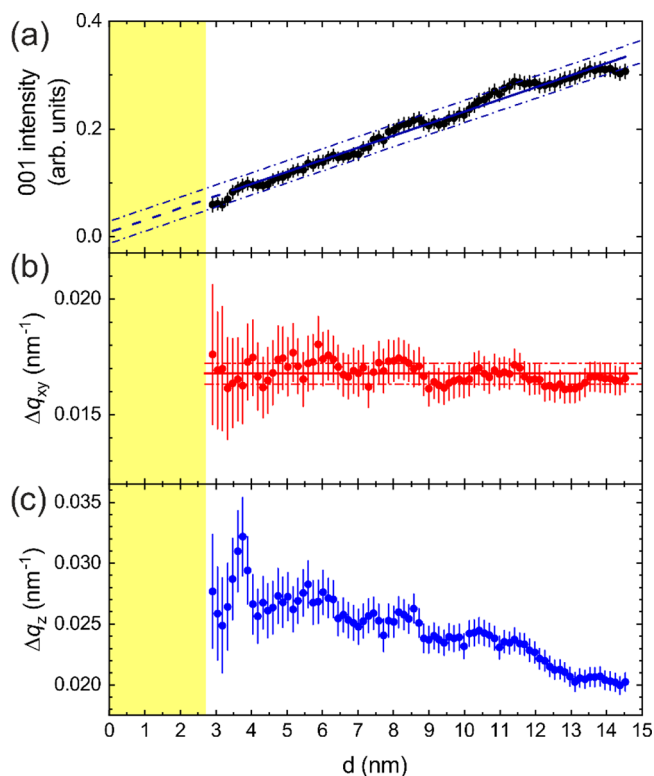


Figure 3. Integral intensity (a) as well as peak width Δq_{xy} (b) and Δq_z (c) of the (001) diffraction as a function of film thickness.

its widths, Δq_z , Δq_{xy} (fwhm's), along the q_z and q_{xy} directions, respectively. The volume of the “lying-down” PEN phase is directly proportional to the integral intensity of the (001) diffraction. The measured (001) intensity evidenced a linear growth of the “lying-down” PEN phase as confirmed by a linear fit. The shaded area in Figure 3 indicates the inaccessible range for reliable fitting of the (001) diffraction spot due to a very low diffracted intensity. The principal limitation is the beam damage threshold, which was found to be approximately 10^{11} photons/s in our geometry. This photon flux induces damage to graphene, which can be observed in the growth of “standing-up” PEN phase instead of the “lying-down” phase. The extrapolation with the corresponding confidence interval toward the nucleation regime indicates a constant growth rate of one single PEN phase from the very beginning of the deposition process.

The diffracted intensity profile in q -space was fitted with a two-dimensional Gaussian function having two independent widths (fwhm's), Δq_z and Δq_{xy} . The lateral width, Δq_{xy} , of the (001) diffraction spot displays only statistical deviations around the mean value of 0.017 \AA^{-1} , shown as a red line in Figure 3 (the dashed lines show the standard deviation). This value merely reflects the width of the instrumental function, as it is broadened by the projected surface area of the SiC sample used in the GIWAXS experiment. In contrast, the Δq_z width of the (001) reflection, which is oriented perpendicular to the

graphene surface, shows gradually decreasing width and is slowly approaching the instrumental limit of 0.018 \AA^{-1} . Using the Scherrer formula and a Gaussian deconvolution, we can estimate the mean vertical correlation length $\Lambda_z = 2\pi/\sqrt{\Delta q_z^2 - \Delta q_1^2}$, where Δq_1 is the measured instrumental function along the q_z direction. The Λ_z of PEN crystals increases from 25 to almost 44 nm for a thickness between 3.8 and 12 nm, respectively. These values correlate with the height of PEN crystals determined by AFM analysis as given later in text.

Confocal Raman Mapping (CRM). An independent view of the crystallographic orientation of single crystal PEN islands on SiC seeded graphene in direct space is provided by ex situ polarized Raman spectroscopy.⁵⁹ The polarized excitation and detection of Raman scattering for PEN was recently used to assess the orientation of PEN films on exfoliated and CVD graphene.⁶⁰ Here, we extend the polarized CRM analysis to epitaxial graphene and validate in real space the GIWAXS observations presented in the previous paragraph. In our analysis, we focus on the two characteristic aromatic C–C stretching modes^{61,62} located at 1373 cm^{-1} (A_g) and 1598 cm^{-1} (B_{3g}), which can be assigned to the short and long axis vibration modes of PEN, respectively. For spatial mapping of PEN crystals, it is practical to define the parameter $P = (I_S - I_L)/(I_S + I_L)$ describing the degree of molecular orientation, where I_S and I_L are the integral intensities of the short and long axis vibration bands, respectively. If we assume a polarized and collinear excitation and detection of Raman spectra with the electric field vector E aligned along a specific crystallographic direction, a value of $P = +1$ implies a perfect orientation of the short molecular axis along this selected crystallographic direction in the probed confocal volume. On the other hand, the negative value $P = -1$ would indicate a complete orientation of the long molecular axis along this chosen crystallographic direction, whereas P values close to zero point to randomly oriented PEN molecules in the probed volume. Figure 4a shows the confocal Raman map of P overlaid on a bright field microscopy image of a single PEN island.

The homogeneous distribution ($P \approx +1$) across the whole scanned PEN island clearly indicates the existence of a single

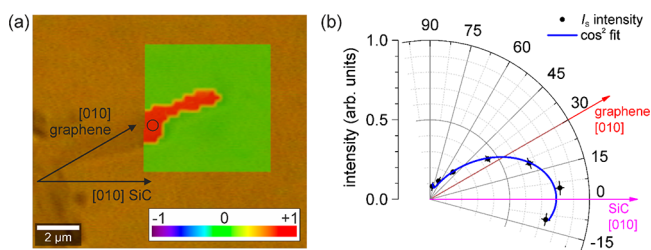


Figure 4. (a) Overlap of the optical microscopy image and confocal Raman mapping. The orientation parameter P (with the scale from -1 to 1) based on confocal Raman mapping (CRM) of the single crystal PEN island. The polarization of exciting and detected radiation was set collinear with the $[010]$ direction of SiC substrate. The macroscopic long axis of the PEN crystal is oriented along the $[010]$ graphene direction. The black circle indicates the probed area where a full molecular orientation analysis as shown in (b) was performed. The polar graph of Raman band integral intensity I_s (1373 cm^{-1}) as a function of angle between the exciting laser field E and the $[010]$ direction of the SiC substrate. The blue line shows a cosine square fit to experimental data.

PEN crystal with the short molecular axis approximately aligned along $[010]$ direction of the underlying SiC substrate. The area surrounding the PEN crystal yields $P = 0$ (green color in Figure 4a), because both intensities, I_S and I_L , are zero outside of the PEN crystal. A detailed molecular orientation analysis performed at a single spot is shown in Figure 4b. The polarization of the excitation laser E field was successively rotated in 15° steps with respect to the $[010]$ direction of the SiC substrate. The scattered Raman signal having the polarization collinear with the excitation E field was recorded (Figure S3). The integral intensity I_S , which belongs to the C–C stretching mode of the short molecular axis, follows the theoretical cosine squared dependence,⁶⁰ which is a clear manifestation of a fully oriented single PEN crystal.

AFM. Before proceeding further with the analysis of our real-time GISAXS experiments, we present the ex situ AFM measurements at various growth stages that will support the interpretation and understanding of the GISAXS reciprocal space measurements. Figure 5a shows the PEN thin film

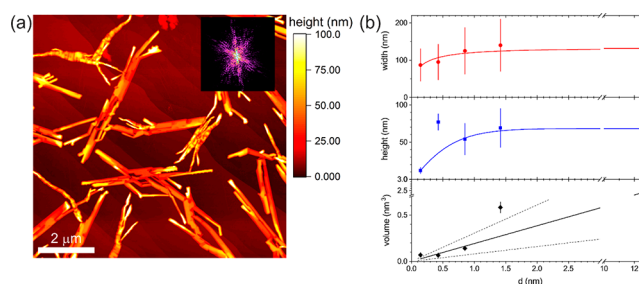


Figure 5. (a) AFM image of PEN crystals at the deposited thickness of 15 nm at a substrate temperature of 50°C . The inset shows the FFT image. (b) Ex situ AFM-based statistical analysis of width, height, and volume of PEN crystals as a function of deposited thickness.

morphology at a deposited thickness of 15 nm and a substrate temperature of 50°C . The azimuthal orientation of the PEN crystallites is in line with the six-fold symmetry of underlying graphene,^{10,13} which is also shown in the FFT of the AFM (inset in Figure 5a).

The nucleation density of PEN crystals is low (Figure 5a), and the mean distance between the individual crystals is in the micrometer range, which prevents the observation of interisland correlations in conventional GISAXS geometries, and dedicated ultrasmall-angle X-ray scattering has to be employed.⁶³ In the first growth phase, PEN molecules on the graphene surface serve as the nucleation template for macroscopic PEN crystals.^{7,8,14,30} The submonolayer PEN film is still present between the PEN crystals shown in Figure 5a. An AFM scan taken with a higher spatial resolution is given in Figure S4. The highly anisotropic crystal shape can be characterized by a set of three parameters: width, length, and height; where the width and length are the average dimensions along the short and long axes of the PEN islands, respectively. As already pointed out in the GIWAXS analysis of the PEN crystals, the six equivalent growth directions are identical with the six independent zigzag directions of the graphene lattice (Figure 6). The very dissimilar surface energies^{64,65} of different crystallographic planes of the PEN crystal are responsible for the observed highly anisotropic growth of PEN islands. Figure 5b shows the average width, height, and volume of PEN crystals as a function of deposited thickness as determined by ex situ AFM measurements. While the volume of the PEN crystals grows

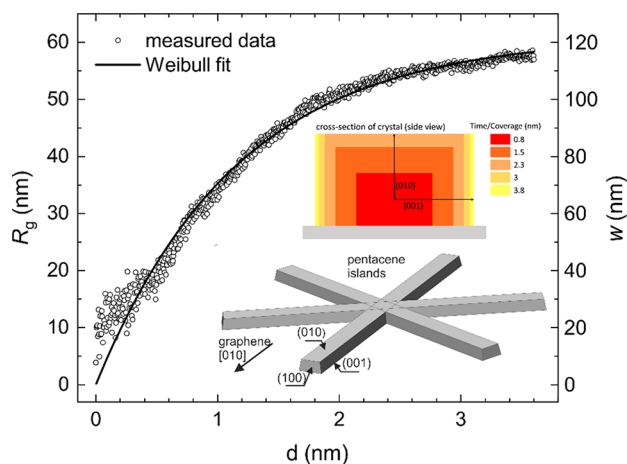


Figure 6. R_g of the growing PEN islands as a function of deposited thickness at a substrate temperature of $T = 50$ °C. Inset shows the sketch of PEN crystal cross section with rapid and quickly saturating growth along the (001) and (010) facets based on GISAXS and AFM data. The second inset sketch describes the PEN crystal facet orientation with respect to underlying graphene. The long and short axes of macroscopic PEN crystals are aligned the zigzag and armchair graphene directions, respectively.

linearly with deposited thickness as expected, the crystal width as well as the height saturates already at 1.5 nm. The relatively large height of individual PEN islands even at a low surface coverages as shown in Figure 5b is not surprising due to a low nucleation surface density of the large PEN crystals. The calculated surface energies⁶⁴ for the (001), (010), and (100) planes are 3.1, 4.8, and 6.4 meV/Å², respectively. The much lower surface energy of (001) facets favors a rapid crystal growth along the (100) facets having the highest surface energy, whereas the existing step barrier and smaller surface energy for (010) facets saturate the vertical growth as well. In spite of the fact that the PEN islands are like nanorods in shape, their size distribution exhibits a large dispersion as can be judged from the error bars in Figure 5b. The ex situ AFM measurements offer valuable insights into the PEN crystal growth on graphene but cannot provide the advantages of in situ real-time GISAXS,⁴⁷ which gives us a better understanding of the kinetics of crystal growth.

The already presented ex situ AFM and polarized CRM measurements confirm the growth of single crystal PEN islands with highly anisotropic shapes having their long axis aligned along the six equivalent zigzag directions of graphene (Figures S2 and S3). In the simultaneous GISAXS/GIWAXS measurements, the observation of the (001) diffraction requires a careful positioning of the graphene substrate with respect to the incoming X-ray beam in order to satisfy the Bragg condition. Depending on the X-ray wavelength employed in the laboratory and at the synchrotron, the in-plane Bragg angle is in the range of ± 2 – 3° from the zigzag graphene direction (Figure 2). This minor displacement of the incoming X-ray beam from the zigzag graphene direction and the corresponding long axis of the crystals enables real-time tracking of the PEN crystal width. The low nucleation density of PEN crystals moves the characteristic interisland interference signature of the GISAXS pattern⁴⁸ into the low q -range, which is inaccessible with our standard GISAXS setup with a resolution limit of approximately 500 nm in real space. Hence, the recorded GISAXS signal is proportional to the average of form factors (FFs)⁴⁸ of many

PEN islands. Moreover, the scattered X-ray intensity of the PEN islands FFs rotated by $\pm 60^\circ$ with respect to incoming X-ray beam will contribute in the low q -range yet again due to rapid crystal growth along (100) crystal facets. The typical aspect ratio is approximately 1:10 between the short and long axis of the PEN crystals as judged from AFM (Figure 5). Interference between the FFs of different crystallographic orientations is expected only shortly after nucleation of PEN islands, which was, however, not experimentally observed in our data sets, presumably due to low scattered intensity and the short acquisition times required for real-time GISAXS/GIWAXS measurements. The GISAXS data were evaluated within the framework of a Guinier analysis,⁶⁶ which is described in the Supporting Information.

The growth of the (001) facets of PEN islands in terms of their radius of gyration, R_g , and estimated average island width, w , at 50 °C substrate temperature is shown in Figure 6. The smaller average size of PEN island width has its origin in the selected static q -range used in the Guinier analysis, which inevitably gives an overproportional weight to the smaller islands against the larger islands. This size filtering effect shifts the average value of polydisperse size distributions toward smaller values. To improve the present GISAXS data analysis, experimental data with an enhanced low q -range are required⁶³ along with the refined simulation taking into account the island size dispersion. The kinetics of diffusion limited growth of (001) facets is described by a simple exponential limited growth model shown by full lines in Figure 6. The fitted value of the rate coefficient is given in the Figure S7. In situ real-time GISAXS experiments with three different temperatures have been carried out. Experiments at two different substrate temperatures ($T = 60$ and 80 °C) showed only negligible changes to R_g , which can be explained by effects like increased PEN mobility and finite desorption rate at elevated substrate temperature.

CONCLUSION

The time-resolved study of PEN growth on epitaxial graphene by means of in situ GISAXS/GIWAXS revealed two stages. In the first stage of up to 1.5 nm of PEN, we observe rapid growth of PEN crystals along the (010) and (001) facets. GISAXS measurements using synchrotron radiation with millisecond time resolution revealed a transition to needle-shaped PEN domains, which is shown by a saturation of the two other growth directions ((001) and (010)).

In the second growth stage, height and width of the needle-shaped domains no longer increase in size. Instead, the much higher surface energy of the (100) planes drives a preferential crystal growth along these facets (needle length) at the expense of the width and height of the domains. The (001) integrated intensity increases linearly with time and the extrapolation toward the beginning of deposition points to uninterrupted linear growth of a single “lying-down” phase of PEN on graphene.

Macroscopically, this growth behavior results in highly anisotropic PEN islands having their long axis aligned with the zigzag graphene direction. The ex situ GIWAXS measurements verified a preferential orientation of PEN crystals following the six-fold symmetry of underlying graphene. The c^* axis of the PEN reciprocal unit cell is aligned with the armchair graphene direction. The crystallographic orientation of PEN crystals was confirmed by ex situ real-space studies using polarized Raman microspectroscopy.

Our methodology of studying kinetics of PEN growth on epitaxial graphene can be further extended to other small organic molecules on arbitrary mono- and polycrystalline two-dimensional substrates.

MATERIALS AND METHODS

Deposition of PEN on Epitaxial Graphene. Epitaxially grown graphene on hexagonal 4H-SiC(0001)⁵⁶ (Graphensic, 15 × 15 mm²) served as substrate. Pentacene (Sigma-Aldrich, ≥99.9% purity) was deposited via evaporation from a resistively heated Alumina crucible. The deposition chamber is equipped with a custom-made 360° X-ray beryllium window, which allows realization of grazing-incidence and grazing-exit beam scattering.⁶⁷ The deposition rate was set constant to 1.38 Å/min, calibrated on a Si wafer with native oxide by means of spectroscopic ellipsometry (J.A. Woolam, M-2000), and monitored in real time with a quartz crystal microbalance. Prior to PEN deposition, the SiC/graphene was annealed at 600 °C in order to desorb surface contaminants. The base vacuum pressure was below 2 × 10⁻⁸ mbar. All in situ and ex situ experiments have been carried out on samples grown at 50 °C substrate temperature.

Ex Situ Laboratory Measurements. The ex situ GIWAXS measurements were performed on a custom-designed small-angle laboratory X-ray scattering setup (Bruker AXS, Nanostar) equipped with liquid-metal jet anode X-ray source (Excillum, MetalJet D2+) and two-dimensional hybrid pixel detector (HPD) (Dectris, Pilatus 300 K). The angle of incidence was set to 0.15°, and the X-ray energy was 9.25 keV (Ga K α line). The AFM measurements (Bruker, Dimension Edge) were done in tapping mode using etched silicon probes (Bruker, TESPA-V2). The polarized Raman measurements were performed on a confocal Raman microscope (Witec, Alpha300 R+) fiber-coupled to a spectrophotometer (Witec, UHTS 300) equipped with a blazed grating (600 grooves/mm) and EMCCD camera (Andor, Newton). The excitation laser line (532 nm) was focused onto the sample surface using a 100× (NA = 0.9) objective. A multimode fiber with a core diameter of 50 μ m served as the confocal pinhole. The employed low laser power below 10 μ W was required to limit the laser beam damage to PEN during extended Raman measurements.

In Situ Real-Time GI-SAXS/WAXS Measurements at the ESRF and DESY. The GI-SAXS/WAXS experiments were conducted at beamline ID10 of the synchrotron radiation source ESRF in France. The X-ray energy was set to 9.25 keV, and the angle of incidence was 0.1°. Two hybrid pixel detectors (HPDs), Maxipix (ESRF) and Pilatus 300 K (Dectris), acquired the GIWAXS and GISAXS patterns simultaneously. The integration time for both detectors was set to 60 s. The selected temporal resolution was found not adequate for quickly varying GISAXS after the evaluation of the ESRF data, so the complementary high-repetition rate GI-SAXS/WAXS measurements were performed at beamline P03 of the synchrotron radiation source DESY in Germany. The X-ray energy was set to 11.4 keV at the 0.1° angle of incidence. Similarly, two HPDs, Pilatus 300 K and Pilatus 1M, were used for detection of the GIWAXS and GISAXS signals, respectively. The acquisition time of 100 ms was short enough to capture the initial stage of PEN crystal growth. Initially, the X-ray beam was adjusted along the zigzag graphene direction, which was done by a rotation of 30° from the [010] direction of the SiC substrate (Figure 2). Then, the SiC crystal was further azimuthally rotated until a bright (001) spot from the PEN film appears. This corresponds to an angle of 2–3°, depending on the X-ray wavelength we used. Data processing was carried out using DPDAK,⁶⁸ GIXSGUI,⁶⁹ and self-programmed scripts in MATLAB.

ASSOCIATED CONTENT

Supporting Information

The Supporting Information is available free of charge on the ACS Publications website at DOI: 10.1021/acsanm.8b00473.

GIWAXS of pentacene crystals on epitaxial graphene, confirmation of oriented growth of PEN molecules, allowed orientations of PEN on graphene, orthogonality

of PEN molecule by polarized confocal Raman spectroscopy, indication of “lying-down” PEN molecules by AFM micrograph, Guinier analysis of GISAXS data, comparison of mean PEN islands widths from ex situ AFM with GISAXS measurements, fitted kinetic rate (PDF)

AUTHOR INFORMATION

Corresponding Author

*E-mail: martin.hodas@uni-tuebingen.de.

ORCID

Martin Hodas: 0000-0001-6328-1717

Peter Siffalovic: 0000-0002-9807-0810

Michal Bodík: 0000-0002-6518-7617

Giuliano Duva: 0000-0001-9492-3276

Matej Jergel: 0000-0002-4482-7881

Alexander Hinderhofer: 0000-0001-8152-6386

Notes

The authors declare no competing financial interest.

ACKNOWLEDGMENTS

We thank Prof. Bernd Schönfeld for providing UHV equipment. We acknowledge support of the APVV-0308-11, APVV-14-0745, APVV-15-0641, APVV-14-0120, and VEGA 2/0092/18. The work was done during implementation of the projects (ITMS 26240220047–25%, ITMS 26240220028–50%) supported by the Research & Development Operational Program funded by the ERDF. We acknowledge financial support of the Deutsche Forschungsgemeinschaft. G.D. acknowledges funding from the Carl Zeiss Stiftung.

REFERENCES

- (1) Geim, A. K.; Novoselov, K. S. The Rise of Graphene. *Nat. Mater.* **2007**, *6*, 183–191.
- (2) Kim, C.-H.; Kymissis, I. Graphene–organic Hybrid Electronics. *J. Mater. Chem. C* **2017**, *5*, 4598–4613.
- (3) Wang, Q. H.; Hersam, M. C. Room-Temperature Molecular-Resolution Characterization of Self-Assembled Organic Monolayers on Epitaxial Graphene. *Nat. Chem.* **2009**, *1*, 206–211.
- (4) Lee, W. H.; Park, J.; Sim, S. H.; Lim, S.; Kim, K. S.; Hong, B. H.; Cho, K. Surface-Directed Molecular Assembly of Pentacene on Monolayer Graphene for High-Performance Organic Transistors. *J. Am. Chem. Soc.* **2011**, *133*, 4447–4454.
- (5) Salzmann, I.; Moser, A.; Oehzelt, M.; Breuer, T.; Feng, X.; Juang, Z. Y.; Nabok, D.; Della Valle, R. G.; Duhm, S.; Heimele, G.; Brillante, A.; Venuti, E.; Bilotti, I.; Christodoulou, C.; Frisch, J.; Puschnig, P.; Draxl, C.; Witte, G.; Müllen, K.; Koch, N. Epitaxial Growth of π -Stacked Perfluoropentacene on Graphene-Coated Quartz. *ACS Nano* **2012**, *6*, 10874–10883.
- (6) Hlawacek, G.; Khokhar, F. S.; van Gastel, R.; Poelsema, B.; Teichert, C. Smooth Growth of Organic Semiconductor Films on Graphene for High-Efficiency Electronics. *Nano Lett.* **2011**, *11*, 333–337.
- (7) Chhikara, M.; Pavlica, E.; Matković, A.; Beltaos, A.; Gajić, R.; Bratina, G. Pentacene on Graphene: Differences between Single Layer and Bilayer. *Carbon* **2014**, *69*, 162–168.
- (8) Jung, W.; Oh, D.-H.; Song, I.; Shin, H.-C.; Ahn, S. J.; Moon, Y.; Park, C.-Y.; Ahn, J. R. Influence of Graphene-Substrate Interactions on Configurations of Organic Molecules on Graphene: Pentacene/epitaxial graphene/SiC. *Appl. Phys. Lett.* **2014**, *105*, 071606.
- (9) Singha Roy, S.; Bindl, D. J.; Arnold, M. S. Templating Highly Crystalline Organic Semiconductors Using Atomic Membranes of Graphene at the Anode/Organic Interface. *J. Phys. Chem. Lett.* **2012**, *3*, 873–878.

- (10) Kim, K.; Santos, E. J. G.; Lee, T. H.; Nishi, Y.; Bao, Z. Epitaxially Grown Strained Pentacene Thin Film on Graphene Membrane. *Small* **2015**, *11*, 2037–2043.
- (11) Jo, S. B.; Kim, H. H.; Lee, H.; Kang, B.; Lee, S.; Sim, M.; Kim, M.; Lee, W. H.; Cho, K. Boosting Photon Harvesting in Organic Solar Cells with Highly Oriented Molecular Crystals via Graphene–Organic Heterointerface. *ACS Nano* **2015**, *9*, 8206–8219.
- (12) Zhang, L.; Roy, S. S.; Safron, N. S.; Shearer, M. J.; Jacobberger, R. M.; Saraswat, V.; Hamers, R. J.; Arnold, M. S.; Andrew, T. L. Orientation Control of Selected Organic Semiconductor Crystals Achieved by Monolayer Graphene Templates. *Adv. Mater. Interfaces* **2016**, *3*, 1600621.
- (13) Nguyen, N. N.; Jo, S. B.; Lee, S. K.; Sin, D. H.; Kang, B.; Kim, H. H.; Lee, H.; Cho, K. Atomically Thin Epitaxial Template for Organic Crystal Growth Using Graphene with Controlled Surface Wettability. *Nano Lett.* **2015**, *15*, 2474–2484.
- (14) Kratzer, M.; Teichert, C. Thin Film Growth of Aromatic Rod-like Molecules on Graphene. *Nanotechnology* **2016**, *27*, 292001.
- (15) Huang, H.; Huang, Y.; Wang, S.; Zhu, M.; Xie, H.; Zhang, L.; Zheng, X.; Xie, Q.; Niu, D.; Gao, Y. Van Der Waals Heterostructures between Small Organic Molecules and Layered Substrates. *Crystals* **2016**, *6*, 113.
- (16) Kowarik, S.; Broch, K.; Hinderhofer, A.; Schwartzberg, A.; Ossó, J. O.; Kilcoyne, D.; Schreiber, F.; Leone, S. R. Crystal Grain Orientation in Organic Homo- and Heteroepitaxy of Pentacene and Perfluoropentacene Studied with X-Ray Spectromicroscopy. *J. Phys. Chem. C* **2010**, *114*, 13061–13067.
- (17) Anger, F.; Ossó, J. O.; Heinemeyer, U.; Broch, K.; Scholz, R.; Gerlach, A.; Schreiber, F. Photoluminescence Spectroscopy of Pure Pentacene, Perfluoropentacene, and Mixed Thin Films. *J. Chem. Phys.* **2012**, *136*, 054701.
- (18) Hinderhofer, A.; Heinemeyer, U.; Gerlach, A.; Kowarik, S.; Jacobs, R. M. J.; Sakamoto, Y.; Suzuki, T.; Schreiber, F. Optical Properties of Pentacene and Perfluoropentacene Thin Films. *J. Chem. Phys.* **2007**, *127*, 194705.
- (19) Alonso, M. I.; Garriga, M.; Karl, N.; Ossó, J. O.; Schreiber, F. Anisotropic Optical Properties of Single Crystalline PTCDA Studied by Spectroscopic Ellipsometry. *Org. Electron.* **2002**, *3*, 23–31.
- (20) Ossó, J. O.; Schreiber, F.; Kruppa, V.; Dosch, H.; Garriga, M.; Alonso, M. I.; Cerdeira, F. Controlled Molecular Alignment in Phthalocyanine Thin Films on Stepped Sapphire Surfaces. *Adv. Funct. Mater.* **2002**, *12*, 455–460.
- (21) Heinemeyer, U.; Scholz, R.; Gisslén, L.; Alonso, M. I.; Ossó, J. O.; Garriga, M.; Hinderhofer, A.; Kytka, M.; Kowarik, S.; Gerlach, A.; Schreiber, F. Exciton-Phonon Coupling in Diindenoperylene Thin Films. *Phys. Rev. B: Condens. Matter Mater. Phys.* **2008**, *78*, 085210.
- (22) Belova, V.; Beyer, P.; Meister, E.; Linderl, T.; Halbich, M. U.; Gerhard, M.; Schmidt, S.; Zechel, T.; Meisel, T.; Generalov, A. V.; Anselmo, A. S.; Scholz, R.; Konovalov, O.; Gerlach, A.; Koch, M.; Hinderhofer, A.; Opitz, A.; Brütting, W.; Schreiber, F. Evidence for Anisotropic Electronic Coupling of Charge Transfer States in Weakly Interacting Organic Semiconductor Mixtures. *J. Am. Chem. Soc.* **2017**, *139*, 8474–8486.
- (23) Kim, J. S.; Kim, B. J.; Choi, Y. J.; Lee, M. H.; Kang, M. S.; Cho, J. H. An Organic Vertical Field-Effect Transistor with Underside-Doped Graphene Electrodes. *Adv. Mater.* **2016**, *28*, 4803–4810.
- (24) Nakayama, Y.; Mizuno, Y.; Hosokai, T.; Koganezawa, T.; Tsuruta, R.; Hinderhofer, A.; Gerlach, A.; Broch, K.; Belova, V.; Frank, H.; Yamamoto, M.; Niederhausen, J.; Glowatzki, H.; Rabe, J. P.; Koch, N.; Ishii, H.; Schreiber, F.; Ueno, N. Epitaxial Growth of an Organic P–n Heterojunction: C60 on Single-Crystal Pentacene. *ACS Appl. Mater. Interfaces* **2016**, *8*, 13499–13505.
- (25) Lee, W. H.; Park, J.; Sim, S. H.; Lim, S.; Kim, K. S.; Hong, B. H.; Cho, K. Surface-Directed Molecular Assembly of Pentacene on Monolayer Graphene for High-Performance Organic Transistors. *J. Am. Chem. Soc.* **2011**, *133*, 4447–4454.
- (26) Wang, C.; Liu, X.; Wang, C.; Xu, X.; Li, Y.; Xie, F.; Gao, Y. Molecular Orientation of Copper Phthalocyanine Thin Films on Different Monolayers of Fullerene on SiO₂ or Highly Oriented Pyrolytic Graphite. *Appl. Phys. Lett.* **2015**, *106*, 121603.
- (27) Chen, W.; Huang, H.; Thye, A.; Wee, S. Molecular Orientation Transition of Organic Thin Films on Graphite: The Effect of Intermolecular Electrostatic and Interfacial Dispersion Forces. *Chem. Commun.* **2008**, *36*, 4276.
- (28) Koch, N.; Vollmer, A.; Salzmann, I.; Nickel, B.; Weiss, H.; Rabe, J. P. Evidence for Temperature-Dependent Electron Band Dispersion in Pentacene. *Phys. Rev. Lett.* **2006**, *96*, 156803.
- (29) Götzen, J.; Käfer, D.; Wöll, C.; Witte, G. Growth and Structure of Pentacene Films on Graphite: Weak Adhesion as a Key for Epitaxial Film Growth. *Phys. Rev. B: Condens. Matter Mater. Phys.* **2010**, *81*, 085440.
- (30) Hlawacek, G.; Khokhar, F. S.; van Gestel, R.; Zandvliet, H. J. W.; Poelsema, B.; Teichert, C. In-Situ Observation of Organic Thin Film Growth on Graphene. In *Small Organic Molecules on Surfaces: Fundamentals and Applications*; Sitter, H., Draxl, C., Ramsey, M., Eds.; Springer, 2013; pp 107–139.
- (31) Forcker, R.; Gruenewald, M.; Fritz, T. Optical Differential Reflectance Spectroscopy on Thin Molecular Films. *Annu. Rep. Prog. Chem., Sect. C: Phys. Chem.* **2012**, *108*, 34.
- (32) Kytka, M.; Gerlach, A.; Schreiber, F.; Kováč, J. Real-Time Observation of Oxidation and Photo-Oxidation of Rubrene Thin Films by Spectroscopic Ellipsometry. *Appl. Phys. Lett.* **2007**, *90*, 131911.
- (33) Heinemeyer, U.; Broch, K.; Hinderhofer, A.; Kytka, M.; Scholz, R.; Gerlach, A.; Schreiber, F. Real-Time Changes in the Optical Spectrum of Organic Semiconducting Films and Their Thickness Regimes during Growth. *Phys. Rev. Lett.* **2010**, *104*, 257401.
- (34) Yoshida, H.; Inaba, K.; Sato, N. X-Ray Diffraction Reciprocal Space Mapping Study of the Thin Film Phase of Pentacene. *Appl. Phys. Lett.* **2007**, *90*, 181930.
- (35) Kowarik, S.; Gerlach, A.; Sellner, S.; Schreiber, F.; Cavalcanti, L.; Konovalov, O. Real-Time Observation of Structural and Orientational Transitions during Growth of Organic Thin Films. *Phys. Rev. Lett.* **2006**, *96*, 125504.
- (36) Kowarik, S.; Gerlach, A.; Schreiber, F. Organic Molecular Beam Deposition: Fundamentals, Growth Dynamics, and *in Situ* Studies. *J. Phys.: Condens. Matter* **2008**, *20*, 184005.
- (37) Watanabe, T.; Hosokai, T.; Koganezawa, T.; Yoshimoto, N. *In Situ* Real-Time X-Ray Diffraction During Thin Film Growth of Pentacene. *Mol. Cryst. Liq. Cryst.* **2012**, *566*, 18–21.
- (38) Frank, C.; Novák, J.; Gerlach, A.; Ligorio, G.; Broch, K.; Hinderhofer, A.; Aufderheide, A.; Banerjee, R.; Nervo, R.; Schreiber, F. Real-Time X-Ray Scattering Studies on Temperature Dependence of Perfluoropentacene Thin Film Growth. *J. Appl. Phys.* **2013**, *114*, 043515.
- (39) Kowarik, S. Thin Film Growth Studies Using Time-Resolved X-Ray Scattering. *J. Phys.: Condens. Matter* **2017**, *29*, 043003.
- (40) Banerjee, R.; Novák, J.; Frank, C.; Lorch, C.; Hinderhofer, A.; Gerlach, A.; Schreiber, F. Evidence for Kinetically Limited Thickness Dependent Phase Separation in Organic Thin Film Blends. *Phys. Rev. Lett.* **2013**, *110*, 185506.
- (41) Mayer, A. C.; Ruiz, R.; Zhou, H.; Headrick, R. L.; Kazimirov, A.; Malliaras, G. G. Growth Dynamics of Pentacene Thin Films: Real-Time Synchrotron X-Ray Scattering Study. *Phys. Rev. B: Condens. Matter Mater. Phys.* **2006**, *73*, 205307.
- (42) Hong, S.; Amassian, A.; Woll, A. R.; Bhargava, S.; Ferguson, J. D.; Malliaras, G. G.; Brock, J. D.; Engstrom, J. R. Real Time Monitoring of Pentacene Growth on SiO₂ from a Supersonic Source. *Appl. Phys. Lett.* **2008**, *92*, 253304.
- (43) Kowarik, S.; Gerlach, A.; Skoda, M. W. A.; Sellner, S.; Schreiber, F. Real-Time Studies of Thin Film Growth: Measurement and Analysis of X-Ray Growth Oscillations beyond the Anti-Bragg Point. *Eur. Phys. J.: Spec. Top.* **2009**, *167*, 11–18.
- (44) Krause, B.; Schreiber, F.; Dosch, H.; Pimpinelli, A.; Seeck, O. H. Temperature Dependence of the 2D-3D Transition in the Growth of PTCDA on Ag(111): A Real-Time X-Ray and Kinetic Monte Carlo Study. *Europhys. Lett.* **2004**, *65*, 372–378.

- (45) Ruiz, R.; Choudhary, D.; Nickel, B.; Toccoli, T.; Chang, K. C.; Mayer, A. C.; Clancy, P.; Blakely, J. M.; Headrick, R. L.; Iannotta, S.; Malliaras, G. G. Pentacene Thin Film Growth. *Chem. Mater.* **2004**, *16*, 4497–4508.
- (46) Woll, A. R.; Desai, T. V.; Engstrom, J. R. Quantitative Modeling of in Situ X-Ray Reflectivity during Organic Molecule Thin Film Growth. *Phys. Rev. B: Condens. Matter Mater. Phys.* **2011**, *84*, 075479.
- (47) Renaud, G.; Lazzari, R.; Revenant, C.; Barbier, A.; Noblet, M.; Ulrich, O.; Leroy, F.; Jupille, J.; Borensztein, Y.; Henry, C. R.; et al. Real-Time Monitoring of Growing Nanoparticles. *Science* **2003**, *300*, 1416–1419.
- (48) Renaud, G.; Lazzari, R.; Leroy, F. Probing Surface and Interface Morphology with Grazing Incidence Small Angle X-Ray Scattering. *Surf. Sci. Rep.* **2009**, *64*, 255–380.
- (49) Bommel, S.; Kleppmann, N.; Weber, C.; Spranger, H.; Schäfer, P.; Novak, J.; Roth, S. V.; Schreiber, F.; Klapp, S. H. L.; Kowarik, S. Unravelling the Multilayer Growth of the Fullerene C₆₀ in Real Time. *Nat. Commun.* **2014**, *5*, 5388.
- (50) Weidman, M. C.; Smilgies, D. M.; Tisdale, W. A. Kinetics of the Self-Assembly of Nanocrystal Superlattices Measured by Real-Time in Situ X-Ray Scattering. *Nat. Mater.* **2016**, *15*, 775–781.
- (51) Smilgies, D. M.; Li, R.; Giri, G.; Chou, K. W.; Diao, Y.; Bao, Z.; Amassian, A. Look Fast: Crystallization of Conjugated Molecules during Solution Shearing Probed in-Situ and in Real Time by X-Ray Scattering. *Phys. Status Solidi RRL* **2013**, *7*, 177–179.
- (52) Smilgies, D. M. In-Situ Real-Time X-Ray Scattering for Probing the Processing-Structure-Performance Relation. *MRS Online Proc. Libr.* **2014**, *1695*, mrs14-1695-ff07-03.
- (53) Ramana Murty, M. V.; Curcic, T.; Judy, A.; Cooper, B. H.; Woll, A. R.; Brock, J. D.; Kycia, S.; Headrick, R. L. Real-Time X-Ray Scattering Study of Surface Morphology Evolution during Ion Erosion and Epitaxial Growth of Au(111). *Phys. Rev. B: Condens. Matter Mater. Phys.* **1999**, *60*, 16956.
- (54) Ye, M.; Cui, Y. T.; Nishimura, Y.; Yamada, Y.; Qiao, S.; Kimura, A.; Nakatake, M.; Namatame, H.; Taniguchi, M. Edge States of Epitaxially Grown Graphene on 4H-SiC(0001) Studied by Scanning Tunneling Microscopy. *Eur. Phys. J. B* **2010**, *75*, 31–35.
- (55) Schumann, T.; Dubslaff, M.; Oliveira, M. H.; Hanke, M.; Lopes, J. M. J.; Riechert, H. Effect of Buffer Layer Coupling on the Lattice Parameter of Epitaxial Graphene on SiC(0001). *Phys. Rev. B: Condens. Matter Mater. Phys.* **2014**, *90*, 041403.
- (56) Yazdi, R. G.; Iakimov, T.; Yakimova, R. Epitaxial Graphene on SiC: A Review of Growth and Characterization. *Crystals* **2016**, *6*, 53.
- (57) Nabok, D.; Puschnig, P.; Ambrosch-Draxl, C.; Werzer, O.; Resel, R.; Smilgies, D.-M. Crystal and Electronic Structures of Pentacene Thin Films from Grazing-Incidence X-Ray Diffraction and First-Principles Calculations. *Phys. Rev. B: Condens. Matter Mater. Phys.* **2007**, *76*, 235322.
- (58) Mattheus, C. C.; Dros, A. B.; Baas, J.; Meetsma, A.; Boer, J. L. de; Palstra, T. T. M. Polymorphism in Pentacene. *Acta Crystallogr., Sect. C: Cryst. Struct. Commun.* **2001**, *57*, 939–941.
- (59) Presser, V.; Schuster, B.-E.; Casu, M. B.; Heinemeyer, U.; Schreiber, F.; Nickel, K. G.; Chassé, T. Raman Polarization Studies of Highly Oriented Organic Thin Films. *J. Raman Spectrosc.* **2009**, *40*, 2015–2022.
- (60) Chen, C.-Y.; Wong, D. P.; Huang, Y.-F.; Lien, H.-T.; Chiang, P.-C.; Li, P.-L.; Shih, F.-Y.; Wang, W.-H.; Chen, K.-H.; Chen, L.-C.; Chen, Y.-F. Understanding the Interplay between Molecule Orientation and Graphene Using Polarized Raman Spectroscopy. *ACS Photonics* **2016**, *3*, 985–991.
- (61) Cheng, H.-L.; Mai, Y.-S.; Chou, W.-Y.; Chang, L.-R.; Liang, X.-W. Thickness-Dependent Structural Evolutions and Growth Models in Relation to Carrier Transport Properties in Polycrystalline Pentacene Thin Films. *Adv. Funct. Mater.* **2007**, *17*, 3639–3649.
- (62) Brillante, A.; Della Valle, R. G.; Farina, L.; Girlando, A.; Masino, M.; Venuti, E. Raman Phonon Spectra of Pentacene Polymorphs. *Chem. Phys. Lett.* **2002**, *357*, 32–36.
- (63) Müller-Buschbaum, P.; Bauer, E.; Maurer, E.; Roth, S. V.; Gehrke, R.; Burghammer, M.; Riekel, C. Large-Scale and Local-Scale Structures in Polymer-Blend Films: A Grazing-Incidence Ultra-Small-Angle X-Ray Scattering and Sub-Microbeam Grazing-Incidence Small-Angle X-Ray Scattering Investigation. *J. Appl. Crystallogr.* **2007**, *40*, s341–s345.
- (64) Northrup, J. E.; Tiago, M. L.; Louie, S. G. Surface Energetics and Growth of Pentacene. *Phys. Rev. B: Condens. Matter Mater. Phys.* **2002**, *66*, 121404.
- (65) Verlaak, S.; Steudel, S.; Heremans, P.; Janssen, D.; Deleuze, M. S. Nucleation of Organic Semiconductors on Inert Substrates. *Phys. Rev. B: Condens. Matter Mater. Phys.* **2003**, *68*, 195409.
- (66) Svergun, D. I.; Feigin, L. A. *Structure Analysis by Small-Angle X-Ray and Neutron Scattering*; Plenum Press, 1987.
- (67) Ritley, K. A.; Krause, B.; Schreiber, F.; Dosch, H. A Portable Ultrahigh Vacuum Organic Molecular Beam Deposition System for in Situ X-Ray Diffraction Measurements. *Rev. Sci. Instrum.* **2001**, *72*, 1453–1457.
- (68) Benecke, G.; Wagermaier, W.; Li, C.; Schwartzkopf, M.; Flucke, G.; Hoerth, R.; Zizak, I.; Burghammer, M.; Metwalli, E.; Müller-Buschbaum, P.; Trebbin, M.; Förster, S.; Paris, O.; Roth, S. V.; Fratzl, P. IUCr. A Customizable Software for Fast Reduction and Analysis of Large X-Ray Scattering Data Sets: Applications of the New *DPDAK* Package to Small-Angle X-Ray Scattering and Grazing-Incidence Small-Angle X-Ray Scattering. *J. Appl. Crystallogr.* **2014**, *47*, 1797–1803.
- (69) Jiang, Z. IUCr. *GIXSGUI*: A MATLAB Toolbox for Grazing-Incidence X-Ray Scattering Data Visualization and Reduction, and Indexing of Buried Three-Dimensional Periodic Nanostructured Films. *J. Appl. Crystallogr.* **2015**, *48*, 917–926.